Simultaneous in vivo recording of local brain temperature and electrophysiological signals with a novel neural probe

Simultaneous *in vivo* recording of local brain temperature and electrophysiological signals with a novel neural probe

Z. Fekete[1,2], M. Csernai[3], K. Kocsis,[3,4], Á. Cs. Horváth[1,2,5], A. Pongrácz[1,2], P. Barthó[3]

[1]MTA EK NAP B Research Group for Implantable Microsystems, 29-33 Konkoly-Thege st, Budapest, H-1121, Hungary
[2]Institute of Technical Physics & Material Sciences, Centre for Energy Research, Hungarian Academy of Sciences, 29-33 Konkoly-Thege st, Budapest, H-1121, Hungary
[3]MTA TTK NAP B Sleep Oscillations Research Group, Magyar Tudósok krt 2, Budapest, H-1117, Hungary
[4]Faculty of Information Technology & Bionics, Pázmány Péter Catholic University, 50/A Práter st, H-1083, Budapest, Hungary
[5]Óbuda University, 96/B Bécsi ut, Budapest, H-1034, Hungary

Abstract

Temperature is an important factor for neural function both in normal and pathological states, nevertheless, simultaneous monitoring of local brain temperature and neuronal activity has not yet been undertaken. In our work, we propose an implantable, calibrated multimodal biosensor that facilitates the complex investigation of thermal changes in both cortical and deep brain regions, while records multiunit activity of neuronal populations in mice. The fabricated neural probe contains four electrical recording sites and a platinum temperature sensor filament integrated on the same probe shaft within a distance of 30 µm from the closest recording site. The feasibility of the simultaneous functionality is presented in *in vivo* studies. The probe was tested in the thalamus of anesthetized mice while manipulating the core temperature of the animals. We obtained multiunit and local field recordings along with measurement of local brain temperature with accuracy of 0.14 °C. Brain temperature generally followed core body temperature, but also showed superimposed fluctuations corresponding to epochs of increased local neural activity. With the application of higher currents, we increased the local temperature by several degrees without observable tissue damage between 34-39 °C.

1. Introduction

Proper thermoregulation is essential for our everyday functioning, and within that, the temperature of the brain is of paramount importance. The rate of any chemical reaction or process occurring in

the brain depends on temperature, influencing neural activity, the frequency of most EEG rhythms, and cognitive functions (Deboer and Tobler, 1995). Failure of brain temperature regulation can lead to dire consequences such as in heat stroke, whereas induced brain hypothermia can be therapeutic in premature infants or patients with cardiac arrest.

Although body core and brain temperature are correlated within certain limits, brain temperature can fluctuate as much as 2-3 °C during different behavioural conditions, states of alertness, or in response to environmental changes (Delgado and Hanai, 1966; Kovalzon, 1973; McElligott and Melzack, 1967), and even more in response to certain drugs (Kiyatkin, 2010). Neuronal activity is shown to be highly dependent on local temperature changes in the brain (Deboer and Tobler, 1995; Sheroziya and Timofeev, 2015). However, little is known about this genuine neuromodulatory effect, which has great impact on our sleep quality, mood and behaviour.

There is a range of invasive and non-invasive methods to monitor brain temperature. Non-invasive techniques include microwave radiometry (Han et al., 2001), magnetic resonance thermometry (Rieke and Butts Pauly, 2008), ultrasound thermometry (Arthur et al., 2005) and near-infrared spectroscopy (Hollis et al., 2001). All these methods provide adequate accuracy for temperature measurement, however, their limited spatial resolution and bulky experimental setup hinder their use in small animal models like rats or mice, especially in freely moving paradigms.

Several invasive solutions have been recently proposed to monitor local temperature changes when using implantable devices. Kim et al. investigated the effect of integrated circuit heat dissipation on Utah arrays (Kim et al., 2007). Li et al monitored temperature with 0.9 °C accuracy in open-heart surgery with polysilicon resistance based probe (Li et al., 2011). The simultaneous measurement of cerebral blood flow and temperature has been demonstrated by using integrated gold resistance temperature detectors on polyimide foils (Li et al., 2012). Specifically, direct measurements of brain temperature have been performed through intracranially implanted thermistors (Rossi et al., 2001; Kunstetter et al., 2014) or thermo-couples (Kiyatkin et al., 2013). In such cases, when deep brain structures or the intracranial pressure is monitored in parallel, their application is admissible. Nevertheless, the integration of temperature measurement functionality into recording electrodes could reduce tissue damage, and more importantly, the interaction between local brain temperature and instantaneous neuronal activity could be resolved more precisely (Fekete, 2015). Technology of silicon microelectrodes provide a good basis to develop such an intergrated system (Vetter et al., 2004), (Michon et al., 2016), (Márton et al., 2016).

Moreover, functionality of integrated temperature sensors can be combined with local heating applications. Integrated heaters fabricated by micromachining process have been used in several neural applications. Suspended polysilicon microheaters have been proposed for determining probe position during subsequent histological analysis (Chen and Wise, 1997). The heating of integrated LEDs on polymer based optogenetic probes has been analysed by integrated platinum heaters (Kim et al., 2013). However, the combined use of integrated microheaters to control local tissue temperature while recording the neuronal activity simultaneously in mice has not been reported elsewhere.

In this work, we demonstrate the application of a minimally invasive multimodal biosensor, where both neuronal activity and thermal information from deep brain structure can be recorded using a single implantable device. The fabricated thermoelectrode accommodates electrophysiological

recording sites and a platinum filament precisely integrated close to each other on the shaft of a silicon microprobe. In our device, one metallization layer is patterned to fabricate both the temperature sensor/actuator and the recording lines and sites, which is eventually a less expensive way compared to previous devices. The feasibility of the proposed biosensor is shown in *in vivo* acute animal experiments.

2. Materials & Methods

2.1 Biosensor design & fabrication

The fabrication of the thermoelectrode is based on standard silicon MEMS (Micro-electro-mechanical systems) process described in this section and briefly shown in Fig. 1.d. The initial substrate is a 380 µm thick (100) single-crystalline silicon wafer. Silicon wafers were oxidized in wet atmosphere at 1100 °C in order to grow a 50 nm thick thermal SiO_2 layer on the substrate surface. To further isolate the recording sites from the bulk Si, a 300 nm thick low-stress silicon nitride (SiN_x) film was then deposited on top of the SiO_2 by low-pressure chemical vapour deposition (LPCVD) at 830 °C and at a chamber pressure of 200 mTorr. The gas flow rate of H_2SiCl_2 and NH_3 was 160 sccm and 20 sccm, respectively. An sacrificial Al layer was used to define the pattern of the TiO_x/Pt recording sites, temperature monitoring filament and conductor paths via a standard lift-off process. First, the 300 nm thick sacrificial Al layer was deposited by electron beam evaporation. This was followed by the first photolithography using Microposit 1818 photoresist and etching steps defining the inverse pattern of the conductor path. The conductor layer consisted of a 15 nm thick adhesion layer of TiO_x formed by reactive sputtering of Ti in an Ar/O_2 atmosphere (Ar/O2 ratio was 80:20). In the same vacuum cycle, 270 nm thick Pt was sputtered on top of TiO_x. The photoresist together with the overlying TiO_x/Pt layer was removed using acetone. The Al layer was etched away in heated nitric acid, to complete with the lift-off process. In the next step the top passivation layer is formed, 300 nm thick SiN_x layers were deposited using LPCVD at 830°C, respectively. Deposition process of the top passivation layer is the same as that of the bottom SiN film. Contact and bonding sites were defined by additional photolithography (Microposit1818 photoresist) step followed by selective SiO_2 and SiN_x wet etching process in NH_4F buffered HF and phosphorous acid until the total removal of the oxide and nitride layers. The probe shaft was micromachined by dry etching using Bosch recipe in an Oxford Plasmalab System 100 DRIE chamber (Oxford Instruments Plc, UK). Masking layer was standard photoresist on the front side, while the etch stop layers were electron beam evaporated Al film and subsequently spin-coated photoresist. Chamber pressure of DRIE was 30 mTorr. ICP power was set to 750 W. C_4F_8 and SF_6 flow rate were 100 sccm and 150 sccm, respectively. The duration of etch and passivation cycles were 4 and 9 seconds, respectively.

The desired thickness of the probe is 65 µm, so the depth of the DRIE pre-etch was defined as 95 µm (Fekete, 2013). After photoresist mask was removed in acetone, the pre-etched microelectrodes were then ground by DISCO GmbH, Germany. The thinned wafers were first detached from the handle tape by simply laying them upon fully wet lab tissue paper. In the aqueous environment, the capillary forces kept the wafer in fixed position, while the tape was gently removed. The individual

probes were flipped out of the wafers manually by tweezers. Finally, probes were mounted onto custom-made PCBs containing a Preci-Dip connector (PRECI 853-87-026-10-002101) and electrical interconnection between the PCB and the silicon chip was finished using wire-bonding technology.

In order to monitor thermal changes in the close vicinity of the neuronal population under investigation, the integrated platinum temperature sensing filament should be as close to the recording sites as possible. The distance between the filament and the closest recording site is 30. The distances between neighbouring recording sites are 100 µm. The surface area of each recording site is 900 μm^2. Length, width and thickness of the probe shaft are 5 mm, 150 µm and 65 µm, respectively (see Fig. 1a-b).

Note that the temperature sensor is simply created in the conductor layer of the thermoelectrode. This gives the advantage of our fabrication concept, namely there is no need to use further functional layers to define the temperature sensor in addition to the conventional production process of silicon multielectrodes.

2.2. Measurement of the thermal and electrical properties of the multimodal biosensor

2.2.1 Temperature measurement and characterization

To measure the temperature of brain tissue in the close vicinity of the thermoelectrode, we utilize the fact that the resistance of the platinum sensor filament depends on its own temperature. First, thermal properties of this integrated sensor filament were investigated with a four-wire resistance measurement setup using a Keithley 6221 precision current generator and a Keithley 2000MM multimeter (Keithley Instruments Inc, OH, USA). Since the temperature dependence of the resistance of the applied platinum filament is linear in the regime of our *in vivo* experiment, we can simply model this property with a first-order approximation of the Callendar–Van Dusen equation. Here, the temperature coefficient α briefly describes the resistance sensitivity of the sensor in response to the change in temperature ($\Delta T=T-T_0$):

$$R_T = R_0 \cdot (1 + \alpha \cdot \Delta T),$$

where R_T and R_0 are the resistance of the filament at temperature T and T_0 °C, respectively.

These parameters were derived by a calibration procedure with an aluminium-oxide Negative Temperature Coefficient thermistor (NTC, Semitec 223Fu5183-15U004, Mouser Electronics, TX, USA) used as reference. The accuracy (±0.5%) of the reference thermistor provided a ±0.14 °C measurement error in our experiments. During the calibration procedure, we controlled experimental conditions to be similar to that of *in vivo* surgery. We used 50 cl of physiological saline as the measurement medium. Both the NTC thermistor and the thermoelectrode was lowered to the same depth (3.2 mm) as during *in vivo* recordings. The distance between the two sensors was 1 mm. The medium was heated up to 50 °C, and then it was left to cool down to room temperature, while we recorded the voltage of the filament with 20 Hz sampling rate. To avoid artefacts of self-heating, 1 mA DC current was maintained.

Based on the measurements, the temperature of the platinum sensor was estimated by fitting a first-order polynomial on the correlation of the sensor voltage to the actual temperature values of the NTC thermistor measured between 33 and 39 °C in the cooling phase, and then, the temperature coefficient of our integrated platinum filament was calculated based on the parameters of the regression (Fig. 2.b). Seven thermoelectrodes were packaged and tested to produce statistical data. At 33 °C the average ± standard deviation of sensor resistance was R_0 = 335.81 ± 18.22Ω and the temperature coefficient of the platinum filament was α = 1721±99ppm/K (n = 7). Fig. 2.c shows a representative example of the calibration results. The error (calculated as $|T_{thermoel.}-T_{NTC}|$) of all the calibration results were 0.102 ± 0.042 °C.

At 1mA measurement currents there is no observable heating of the device. Nevertheless, we tested the extent of local heating of the tissue by elevating measurement currents beyond 5 mA. We applied a heating and passive cooling intervals of 10 seconds, and recorded the temperature at saturation.

2.2.2 Impedance spectroscopy

The impedance of electrophysiological recording sites was measured by electrochemical impedance spectroscopy (EIS) measurements. The EIS measurements were performed in three electrode compartments using an Ag/AgCl reference electrode and a counter electrode of platinum wire. Physiological saline was used as electrolytes. Reference 600 (Gamry Instruments, PA, USA) potentiostat, Gamry Framework 6.02 and Echem Analyst 6.02 were used for experimental control, data collection and analysis. Experiments were performed in a Faraday cage. The probe signal was sinusoidal, 25 mV RMS.

2.3 Animal preparation & *in vivo* recordings

Male C57/BL6 mice (18-25 g, n=13) were anesthetised with urethane (1.5 g/kg) and placed in a stereotactic apparatus. A craniotomy was made above the ventral posteromedial/lateral nucleus (VPM/VPL) of the thalamus (1.6 mm caudal, 1.7 mm medial from the bregma). The thermoelectrode was lowered into one hemisphere, and we inserted the NTC thermistor in the other hemisphere. The reference electrode was placed in the neck muscles. Electrophysiological recordings were made with our thermoelectrode, while the resistance of the integrated platinum filament was measured simultaneously. Extracellular signals were high-pass filtered (0.1 Hz), amplified at 192x gain, and digitized at 20 kHz sampling rate with 16 bit resolution by an Intan headstage and evaluation board (Intan Technologies Llc., Los Angeles, CA).The two recording systems were synchronized. Action potential spikes were detected from our electrophysiological recordings as negative deflections crossing a set threshold. Smoothed multiunit activity was then created by binarizing the spike trains at 1 kHz, and smoothing with a 3 second long square window.

Before the *in vivo* recordings, the thermoelectrodes were calibrated as described in Sec. 2.2.1. The animals core body temperature was manipulated by a controllable heating pad (RWD instruments, China).

2.4 Local heating protocol

The heating capability of our integrated temperature sensor can be considered as the increase in filament resistance caused by increased driving current. Before performing *in vivo* experiments, we have determined the safety margin of the applicable current to the sensor. In DC mode, exceeding a driving current of 30 mA causes irreversible damage to the platinum filaments, so our heating tests were limited to the range below 15 mA. The heating performance of our thermoelectrode was tested in anaesthetized mice (see Fig. 5.a).

Dissipated heat on the individual sections of the thermoelectrode is determined by their resistance, which can be calculated as follows:

$$R = \rho \cdot \frac{l}{A},$$

where ρ, l and A are the resistivity, length and cross-section of the thin film, respectively. According to our calculations, only 45.2% of the electrical power is converted to heat throughout the meander-like 1 mm long, 4 µm wide sensor structure. The rest is dissipated on the backbone (8.2%, 2 mm long, gradually increasing length from 60 µm up to 200 µm) and along the integrated wiring (5 mm long, 40 µm wide) of the sensor's shaft (46.6%).

Rise time (response time) of the sensor was measured as approximately 400 ms in saline with a GDS-820C oscilloscope (Good Will Instrument Co., Ltd., Taiwan). The decay of temperature can be estimated through Newton's Law of Cooling:

$$\Delta T(t) = \Delta T(0) e^{-\frac{t}{\tau}}.$$

Thermal time constant (τ) of our sensor is 1.808±0.118 seconds in the brain tissue. Therefore, in our experiments we used a min. of 10 seconds measurement intervals at 1 mA measurement current, which exceeds 5τ. This way, we could separately analyze the thermal effects of resistive heating intervals. An exponential was fitted on the measured temperature values from 400 ms after the offset of the heating current. Temperature during heating was estimated by the intersection of the exponential and the offset time of the heating pulse (Fig. 4.b).

2.5 Histology

After the experiments, the animals were overdosed with urethane, perfused through the heart with 0.9% saline solution followed by a perfusion solution consisting of 4% paraformaldehyde, 15% picric acid, and 0.05% glutaradehyde in 0.1 M phosphate buffer. The brains were cut into 60 µm slices in

the coronal plane, and washed in phosphate buffer. Sections were mounted on slides, Nissl-stained, and coverslipped. The tracks of the silicon probe were reconstructed from multiple sections.

3. Results & Discussion

In the following sections, we demonstrate the application of the proposed thermoelectrode and validate the device in terms of its electrical properties, temperature measurement ability, and its capability to heat the surrounding brain tissue.

3.1 Electrical properties

First, the electrical properties of the thermoelectrodes were tested through electrochemical impedance spectroscopy, and the measurement results are shown in Fig. 2.a. The average site impedance at 1 kHz was 769±87 kΩ (n=7), which is in the typical range for silicon electrodes.

Next, the electrophysiological properties of the thermoelectrodes were validated *in vivo* in somatosensory cortex and thalamus of urethane-anesthetised mice (n=13). The probes yielded good local field and multiunit recordings (Fig. 3.a), though, due to the 100 µm distance between the recording sites, single units were separable only occasionally (Fig. 3.b-d). Direct current passed through the thermistor did not influence recording quality at low currents (<cca. 7 mA), therefore recording of neural activity was possible with simultaneous temperature measurement. Higher currents progressively introduced noise into the recording, allowing only for alternating electrophysiological and temperature measurement protocols. Also, currents above 5 mA produced observable heating (see Section 3.3), therefore all the measurements were made using 1 mA direct current.

3.2 Temperature measurement and characterization

The accuracy of our temperature sensor is well represented by the *in vivo* experiments (see Fig. 4.a), where parallel temperature monitoring was performed by a rectal sensor, a contralaterally implanted reference NTC sensor (Semitec) and our thermoelectrode lowered to the VPL/VPM thalamus (depth of 3200 µm) in urethane anesthetized mice. Urethane is known to impair thermal regulation (Malkinson et al., 1993), thus the animals' core temperature can be manipulated in a relatively broad range by external heating, such as the animal heating pad. Fig. 4.a shows three heating / cooling cycles between 34-39 °C. Brain temperature measured by the thermoelectrode matched closely the reading of the NTC sensor, and both followed changes in the core body temperature. Brain temperature was consistently 2.5±0.7 °C below core body temperature, as expected in anesthetised small animals (Kiyatkin and Brown, 2005; Zhu et al., 2004).

Under physiological conditions, variations in brain temperature are much lower than that during the heating/cooling protocol (Wang et al., 2014). Periodic fluctuations in brain state are associated with

small increases in core temperature as well as multiunit activity, even under urethane anaesthesia (Whitten et al., 2009). A spontaneously fluctuating epoch is shown on Fig. 4.b, with no manipulation of body temperature (a slow cooling trend can be observed due to the lack of active heating). Microfluctuations of brain temperature in both hemispheres were associated with changes in multiunit activity. Again, the thermoelectrode measurements precisely followed those of the NTC thermistor, with a precision below 0.2 °C.

As our main contribution in this line of research, we fabricated a single device, which is able to record both local tissue temperature and neural activity simultaneously. According to our measurement data, the quality of electrophysiological recording sites on the thermoelectrode is both suitable for local field measurements as well as for multiunit activity recordings. Moreover, the precision of the integrated thermal sensor is excellent for investigating local microfluctuations, as it can distinguish temperature differences smaller than 0.2°C.

3.3. Local heating of brain tissue

Manipulation of the core body temperature can induce global changes, interfering with the study of local thermal changes. Therefore we set out to locally heat the brain tissue by passing larger currents (5 mA or above) through our thermoelectrode. To achieve this, we applied 50 s long heating pulses interleaved with 10 s long epochs of 1 mA measuring current (Fig. 5.a). Since after the offset of the heating current temperature started to decay immediately, we estimated the heated temperature by fitting an exponential on the temperature decay curve (Fig. 5.b., for detailed methods see 2.4). Our *in vivo* results imply that 10 mA of heating current makes a temperature difference of 5.2±0.3 °C (Fig. 5.c), which is adequate to investigate the temperature dependence of neural activity as observed on Fig. 5.a,c. Based on histological evaluation of Nissl-stained sections, we could not distinguish between insertion induced damage and heat induced damage with respect to a reference electrode track, where no heating cycle was applied. We showed that in the investigated temperature range, no observable tissue damage is induced by heating (Fig. 5.d), which is also confirmed recordings of multiunit activity after several heating periods. Depending on the targeted neural application, our device can deliver local temperature control of the tissue at a reasonable dynamic temperature range and precision. The inset of Fig.5.a shows neural data recorded right at the onset of the heating pulse, which gives evidence on the feasibility of simultaneous neural recording and tissue heating with our proposed device.

Conclusion

This work demonstrated an *in vivo* validation of a calibrated microelectrode biosensor capable of simultaneous recording of extracellular neuronal signals and local changes in brain tissue temperature with accuracy below 0.2 °C. To present the feasibility of the device, we did parallel

recordings of fluctuations in brain temperature and multiunit activity in mice both at constant and varied body temperature. The integrated platinum filament was also tested to heat the surrounding tissue volume. We proved that our device is able to efficiently control local temperature between 34-39 °C. In the investigated temperature range, no heat related tissue damage was observed during histological studies performed after the experiments.

Our biosensor concept is envisioned to open new doors in the investigation of the interdependence of neural activity and local brain temperature inside living subjects. Combining the functionalities in 2D or 3D arrays may facilitate the simultaneous monitoring of temperature and neuronal signalling in different brain regions at high resolution.

Acknowledgement

The authors are thankful to the Hungarian Brain Research Program (KTIA NAP 13-2-2015-0004 for Z.F. and KTIA NAP 13-2-2014-0016 for P.B), NKFIH-119650 for P.B and NKFIH 120143 for Z.F. Anita Pongrácz is grateful for the support of Bolyai János Scholarship granted by the HAS.

References

Arthur, R.M., Straube, W.L., Trobaugh, J.W., Moros, E.G., 2005. Non-invasive estimation of hyperthermia temperatures with ultrasound. Int. J. Hyperthermia 21, 589–600. doi:10.1080/02656730500159103

Chen, J., Wise, K.D., 1997. A silicon probe with integrated microheaters for thermal marking and monitoring of neural tissue. IEEE Trans. Biomed. Eng. 44, 770–4. doi:10.1109/10.605437

Deboer, T., Tobler, I., 1995. Temperature dependence of EEG frequencies during natural hypothermia. Brain Res. 670, 153–156. doi:10.1016/0006-8993(94)01299-W

Delgado, J.M., Hanai, T., 1966. Intracerebral temperatures in free-moving cats. Am. J. Physiol. 211, 755–69.

Fekete, Z., 2013. Technology of ultralong deep brain fluidic microelectrodes combined with etching-before-grinding. Microsyst. Technol. 21, 341–344. doi:10.1007/s00542-013-1985-7

Han, J.W., Van Leeuwen, G.M., Mizushina, S., Van de Kamer, J.B., Maruyama, K., Sugiura, T., Azzopardi, D. V, Edwards, A.D., 2001. Monitoring of deep brain temperature in infants using multi-frequency microwave radiometry and thermal modelling. Phys. Med. Biol. 46, 1885–903.

Hollis, V.S., Binzoni, T., Delpy, D.T., 2001. <title>Noninvasive monitoring of brain tissue temperature by near-infrared spectroscopy</title>, in: Chance, B., Alfano, R.R., Tromberg, B.J., Tamura, M., Sevick-Muraca, E.M. (Eds.), Proceedings of the SPIE. pp. 470–481. doi:10.1117/12.434506

Kim, S., Tathireddy, P., Normann, R.A., Solzbacher, F., 2007. Thermal impact of an active 3-D microelectrode array implanted in the brain. IEEE Trans. Neural Syst. Rehabil. Eng. 15, 493–501. doi:10.1109/TNSRE.2007.908429

Kim, T., McCall, J.G., Jung, Y.H., Huang, X., Siuda, E.R., Li, Y., Song, J., Song, Y.M., Pao, H.A., Kim, R.-H., Lu, C., Lee, S.D., Song, I.-S., Shin, G., Al-Hasani, R., Kim, S., Tan, M.P., Huang, Y., Omenetto, F.G., Rogers, J.A., Bruchas, M.R., 2013. Injectable, cellular-scale optoelectronics with applications for wireless optogenetics. Science 340, 211–6. doi:10.1126/science.1232437

Kiyatkin, E. a, 2010. Brain temperature homeostasis: physiological fluctuations and pathological shifts. Front. Biosci. 15, 73–92. doi:10.2741/3608

Kiyatkin, E.A., Brown, P.L., 2005. Brain and body temperature homeostasis during sodium pentobarbital anesthesia with and without body warming in rats. Physiol. Behav. 84, 563–70. doi:10.1016/j.physbeh.2005.02.002

Kovalzon, V.M., 1973. Brain temperature variations during natural sleep and arousal in white rats. Physiol. Behav. 10, 667–70.

Li, C., Wu, P.-M., Hartings, J.A., Wu, Z., Cheyuo, C., Wang, P., LeDoux, D., Shutter, L.A., Ramaswamy, B.R., Ahn, C.H., Narayan, R.K., 2012. Micromachined lab-on-a-tube sensors for simultaneous brain temperature and cerebral blood flow measurements. Biomed. Microdevices 14, 759–68. doi:10.1007/s10544-012-9646-7

Li, K.-S., Chao, T.-Y., Cheng, Y.T., Chen, J.-K., Chen, Y.-S., 2011. Temperature sensing probe integrated with an SU-8 flexible ribbon cable for heart surgery application, in: 2011 16th International Solid-State Sensors, Actuators and Microsystems Conference. IEEE, pp. 2180–2183. doi:10.1109/TRANSDUCERS.2011.5969383

Malkinson, T.J., Veale, W.L., Cooper, K.E., 1993. Experimental characterization and applications of an anesthetized animal model for thermoregulatory investigations. Biomed. Sci. Instrum. 29, 369–76.

Márton, G., Baracskay, P., Cseri, B., Plósz, B., Juhász, G., Fekete, Z., Pongrácz, A., 2016. A silicon-based microelectrode array with a microdrive for monitoring brainstem regions of freely moving rats. J. Neural Eng. 13, 026025. doi:10.1088/1741-2560/13/2/026025

McElligott, J.G., Melzack, R., 1967. Localized thermal changes evoked in the brain by visual and auditory stimulation. Exp. Neurol. 17, 293–312.

Michon, F., Aarts, A., Holzhammer, T., Ruther, P., Borghs, G., McNaughton, B., Kloosterman, F., 2016. Integration of silicon-based neural probes and micro-drive arrays for chronic recording of large populations of neurons in behaving animals. J. Neural Eng. 13, 046018. doi:10.1088/1741-2560/13/4/046018

Rieke, V., Butts Pauly, K., 2008. MR thermometry. J. Magn. Reson. Imaging 27, 376–90. doi:10.1002/jmri.21265

Sheroziya, M., Timofeev, I., 2015. Moderate Cortical Cooling Eliminates Thalamocortical Silent States during Slow Oscillation. J. Neurosci. 35, 13006–13019. doi:10.1523/JNEUROSCI.1359-15.2015

Vetter, R.J., Williams, J.C., Hetke, J.F., Nunamaker, E.A., Kipke, D.R., 2004. Chronic Neural Recording Using Silicon-Substrate Microelectrode Arrays Implanted in Cerebral Cortex. IEEE Trans. Biomed. Eng. 51, 896–904. doi:10.1109/TBME.2004.826680

Wang, H., Wang, B., Normoyle, K.P., Jackson, K., Spitler, K., Sharrock, M., Miller, C.M., Best, C., Llano, D., Du, R., 2014. Brain temperature and its fundamental properties: A review for clinical neuroscientists. Front. Neurosci. 8, 1–17. doi:10.3389/fnins.2014.00307

Whitten, T.A., Martz, L.J., Guico, A., Gervais, N., Dickson, C.T., 2009. Heat synch: inter- and independence of body-temperature fluctuations and brain-state alternations in urethane-anesthetized rats. J. Neurophysiol. 102, 1647–56. doi:10.1152/jn.00374.2009

Zhu, M., Nehra, D., Ackerman, J.J.H., Yablonskiy, D.A., 2004. On the role of anesthesia on the body/brain temperature differential in rats. J. Therm. Biol. 29, 599–603. doi:10.1016/j.jtherbio.2004.08.029

Figure captions

Figure 1. A) Optical microscopy views of a 4-channel microelectrode with integrated platinum temperature sensor filament. B) Perspective scanning electron micrograph of an as-fabricated probe shaft. Scale bar represents 100 µm on each figure. C) Cross-sectional schematic diagram of the main fabrication steps. 1. SiO_2 and SiN_x layer deposition and patterning of platinum wiring 2. Deposition and selective opening of the SiN_x passivation layer. 3. Patterning of front-side Al mask and dry etching of the passivation and insulation layers; evaporation of Al and spin-coating of photoresist to form the backside etch-stop layer. 4. Cross-section of the ready-made probe after removing the masking and etch-stop layers. Left-hand side fully passivated metallization and right-hand side open metallization represent the cross-section of the temperature sensor and the recording site, respectively.

Figure 2. (A) Representative Bode diagram of the four-channel probe. Site identifiers are numbered with respect to the tip. Standard deviation is below 1%, and is therefore not denoted on the figure. B) The thermoelectrode's temperature is calculated from the voltage measured on the sensor (I = 1 mA) and the regression parameters. C) The thermoelectrode's calculated temperature is compared to the respective NTC temperature in the time domain during passive cooling.

Figure 3. Electrophysiological validation of the thermoelectrode. A) Local field and unit activity recorded from VPL/VPM thalamus of a urethane anesthetized mouse on three neighbouring sites. Clusters in feature space (B), spike waveforms (C), auto- and cross-correlograms of the separated neurons (spikes also coloured in A.).

Figure 4. Validation of the thermoelectrode by temperature measurement in vivo A) Parallel changes of core body temperature, brain temperature, and neural activity. Effect of a series of heating cycles between 34-39 °C performed by a heating plate directly placed under urethane anaesthetized mouse. Brain temperature measured by the thermoelectrode strongly coincides with that measured by the NTC thermistor contralaterally. Brain temperature follows body temperature changes within certain bounds, but is generally lower by 2-3 °C. Multiunit activity shows a marked increase on the rising phase of the heating cycle. B). Brain temperature and multiunit activity in an anaesthetized mouse without active heating. Microfluctuations in brain temperature are associated with elevated multiunit activity. Note that the fluctuations are superimposed on a slower and larger cooling trend.

Green line: rectal temperature sensor, black line: contralateral reference NTC thermistor, blue line: temperature sensor of our thermoelectrode. Red curves show the smoothed multiunit activity (arbitrary units) recorded simultaneously by the thermoelectrode.

Figure 5. The thermoelectrode can be used at larger currents to effectively heat brain tissue without damage. A) Example shows heating with 50 seconds long heating pulses at 6 mA, interspersed with measuring current at 1 mA for 10 seconds (black: NTC thermistor temp., blue: thermoelectrode temp., red: thermoelectrode current). Inset: spike triggered multiunit activity right before and after the onset of heating pulse (green arrows). Mean firing actually decreased with heating. B) Temperature could not be directly measured during heating pulses (see 2.4), but was estimated by fitting an exponential on the temperature decay curve after switching from heating to measuring current (marked by the arrowhead). C) Measured temperature difference and multiunit activity after 50 second long heating phase in for various driving currents. Current value of 1 mA was used to measure resting state temperature. Error bars represents SD, p values are always less than 0.05. D) Histology of the electrode track after applying measuring current only (left), and after heating with 6 mA current for 30 minutes (right) in the contralateral hemisphere of the same animal. No heat induced tissue damage can be observed between the two conditions.

Figure 1.

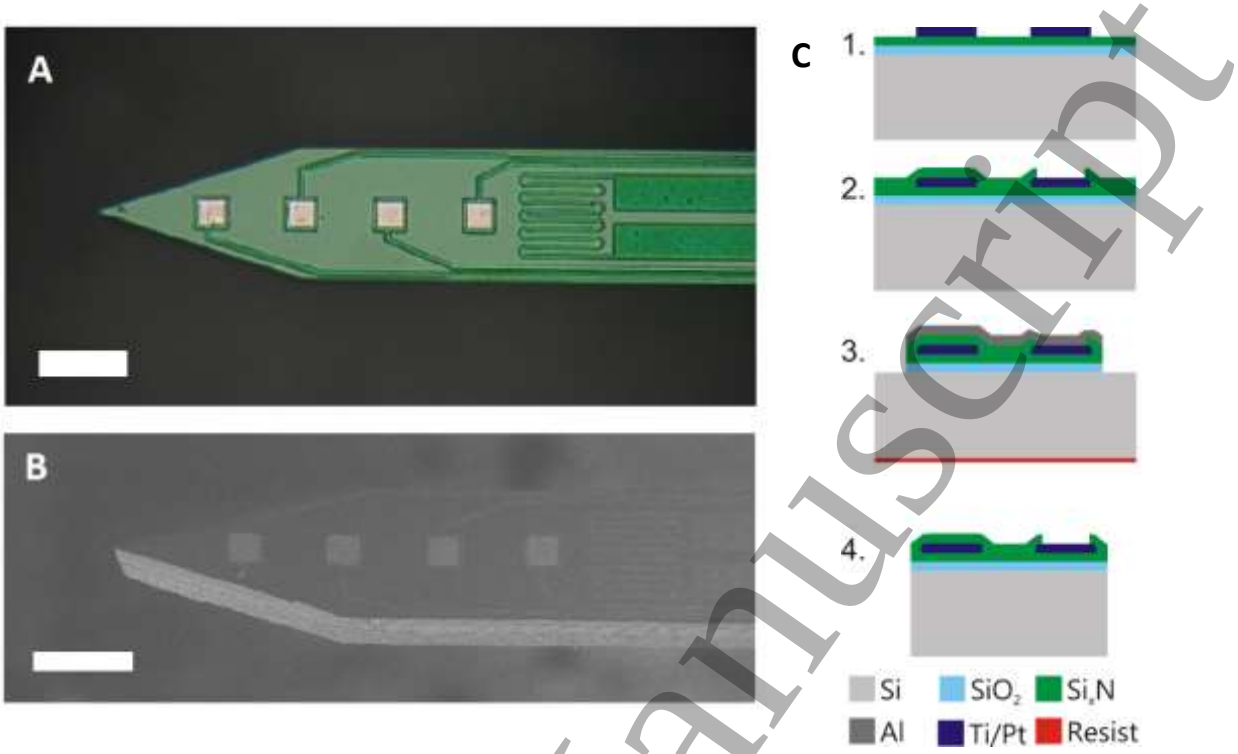

Figure 2

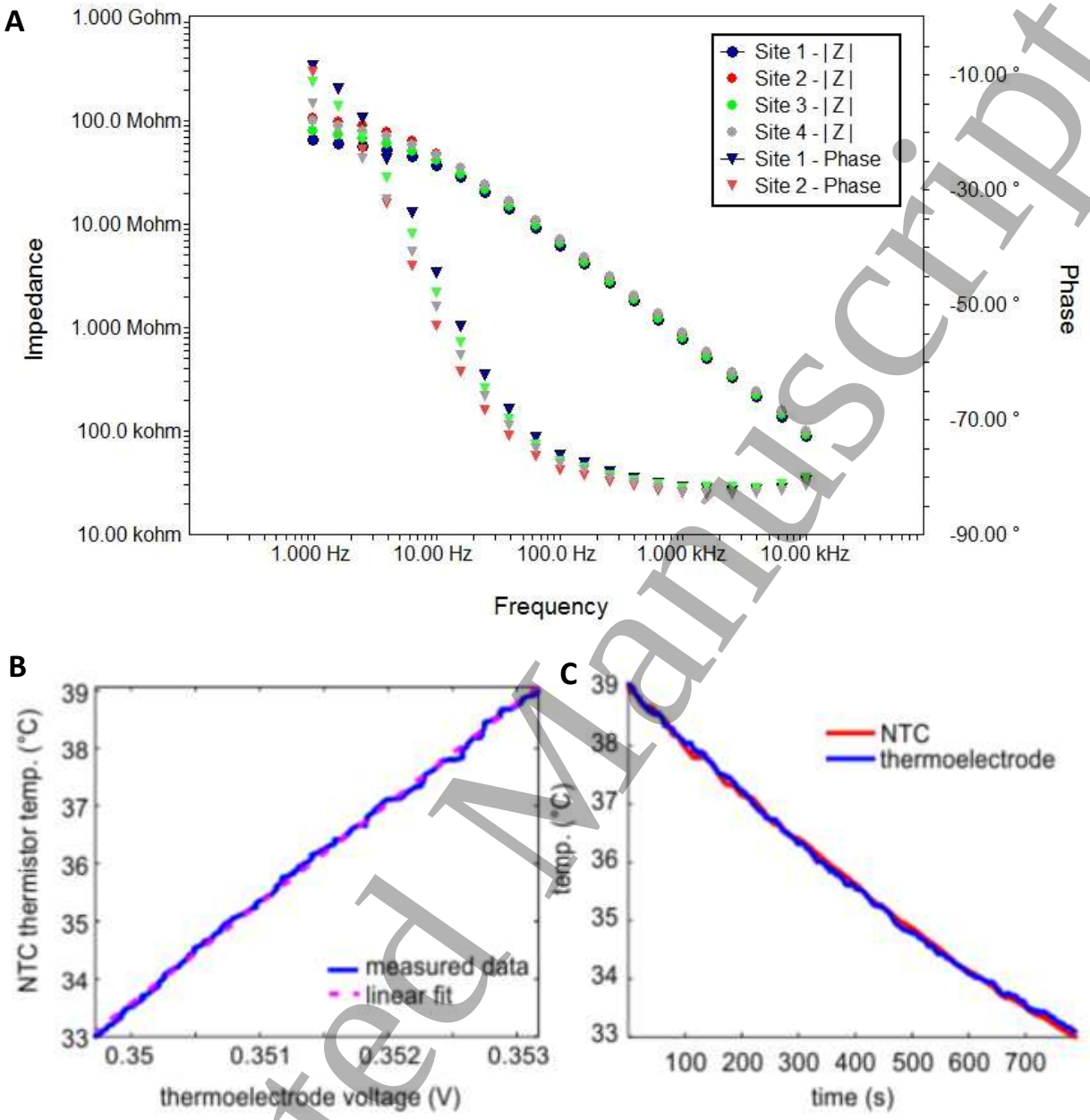

Figure 3

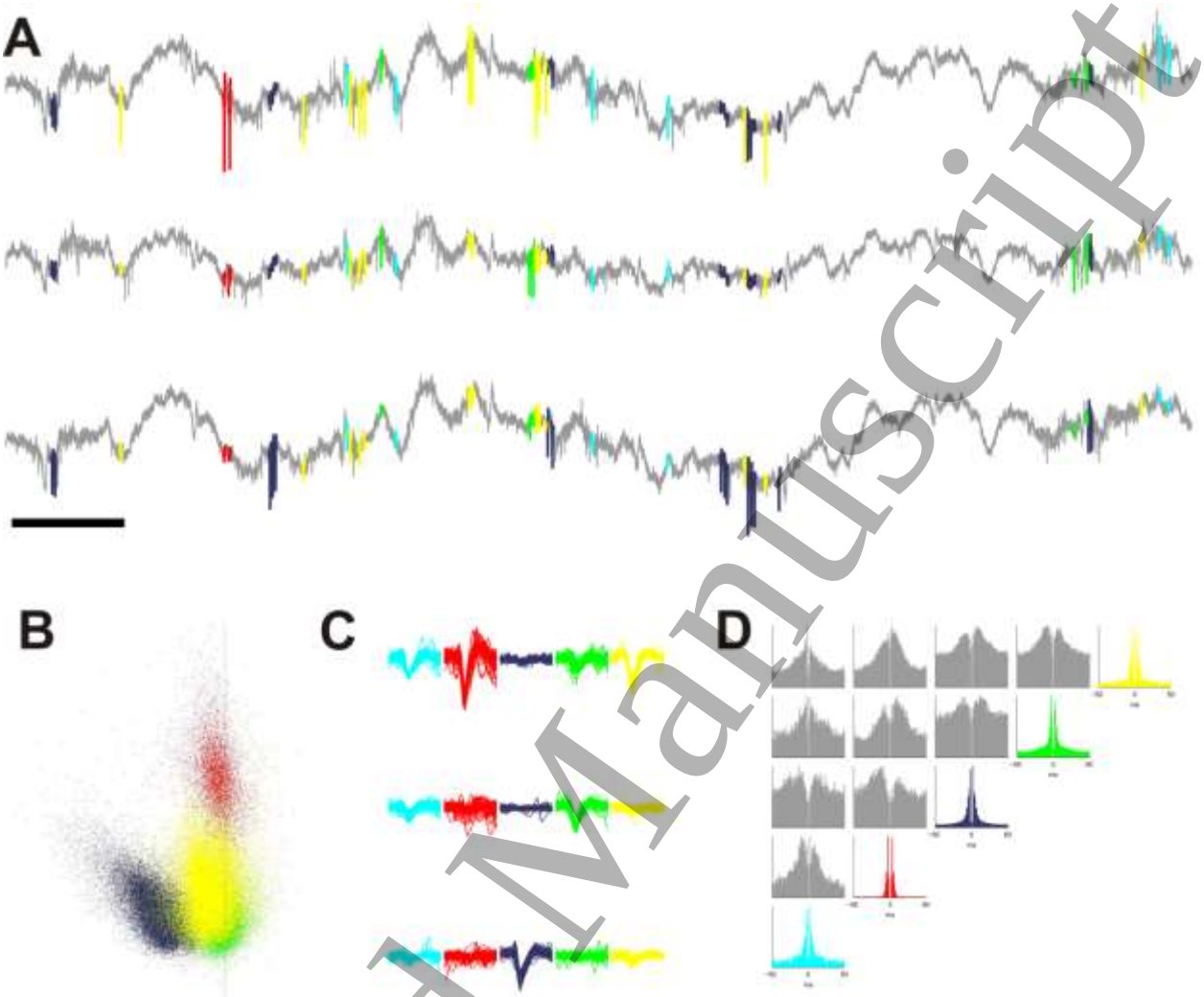

Figure 4.

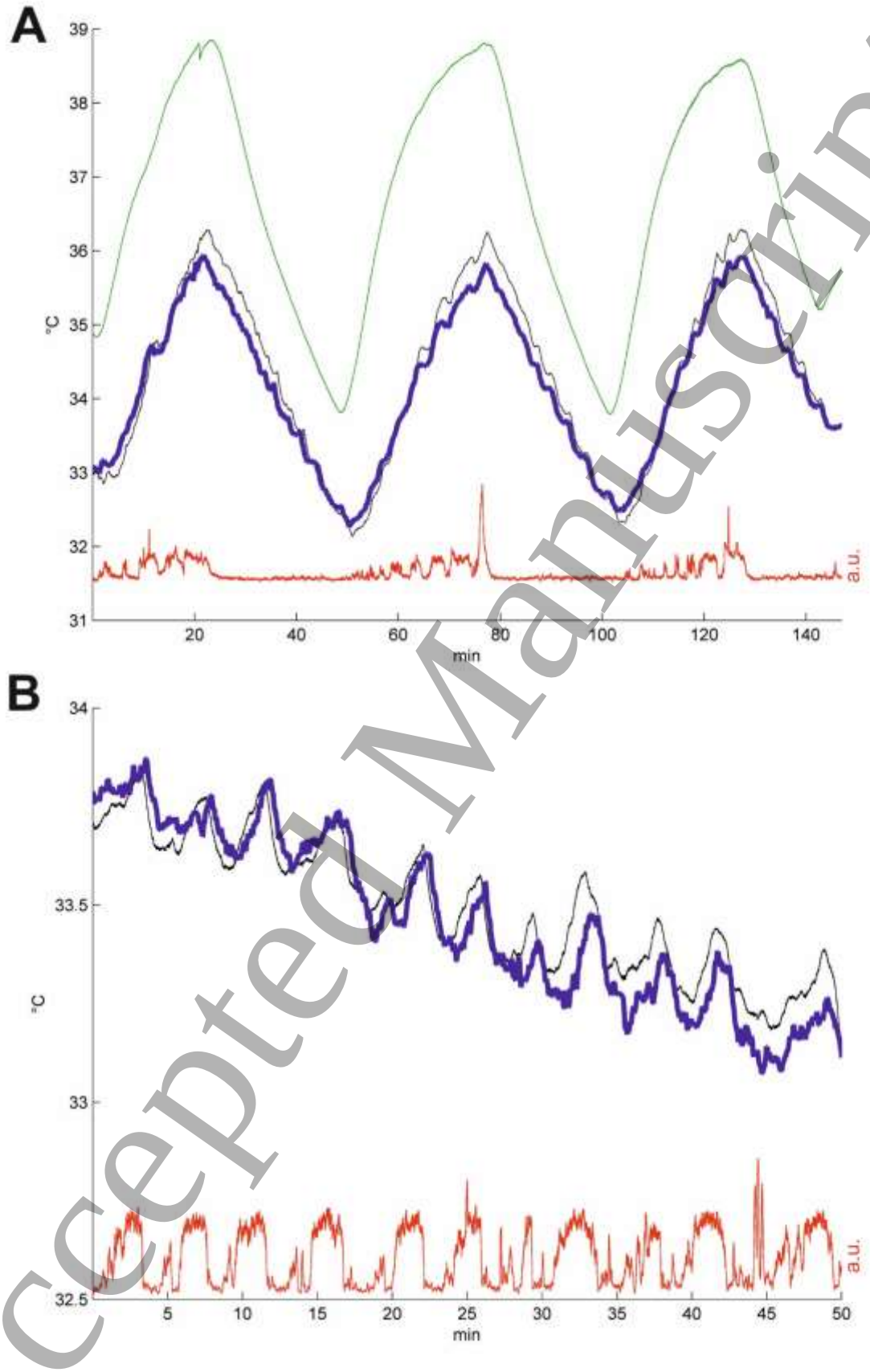

Figure 5.